HHS Public Access

Author manuscript

Nat Immunol. Author manuscript; available in PMC 2016 May 18.

Published in final edited form as:

Nat Immunol. 2016 January ; 17(1): 95–103. doi:10.1038/ni.3313.

Cancer mediates effector T cell dysfunction by targeting microRNAs and EZH2 via glycolysis restriction

Ende Zhao[1,2,11], **Tomasz Maj**[1,11], **Ilona Kryczek**[1], **Wei Li**[1,2], **Ke Wu**[2], **Lili Zhao**[3], **Shuang Wei**[1], **Joel Crespo**[1], **Shanshan Wan**[1], **Linda Vatan**[1], **Wojciech Szeliga**[1], **Irene Shao**[1], **Yin Wang**[1], **Yan Liu**[1], **Sooryanarayana Varambally**[4], **Arul M. Chinnaiyan**[4], **Theodore H. Welling**[1], **Victor E. Marquez**[5], **Jan Kotarski**[6], **Hongbo Wang**[2], **Zehua Wang**[2], **Yi Zhang**[7], **Rebecca Liu**[8], **Guobin Wang**[2], and **Weiping Zou**[1,9,10]

[1]Department of Surgery, University of Michigan School of Medicine, Ann Arbor, MI [2]Departments of Surgery, and Obstetrics and Gynecology, Union Hospital, Tongji Medical College, Huazhong University of Science and Technology, Wuhan, China [3]Department of Biostatistics, University of Michigan School of Medicine, Ann Arbor, MI [4]Department of Pathology, University of Michigan School of Medicine, Ann Arbor, MI [5]Chemical Biology Laboratory, Center for Cancer Research, NCI-Frederick, Frederick, Maryland [6]The First Department of Gynecologic Oncology and Gynecology, Medical University of Lublin, Poland, 20-081 [7]Department of Internal Medicine, University of Michigan School of Medicine, Ann Arbor, MI [8]Department of Obstetrics and Gynecology, University of Michigan School of Medicine, Ann Arbor, MI [9]Graduate Programs in Immunology and Cancer Biology, University of Michigan, Ann Arbor, MI [10]Comprehensive Cancer Center, University of Michigan, Ann Arbor, MI

Abstract

Aerobic glycolysis regulates T cell function. However, if and how primary cancer alters T cell glycolytic metabolism and affects tumor immunity remains a question in cancer patients. Here we report that ovarian cancers imposed glucose restriction on T cells and dampened their function via maintaining high expression of microRNA101 and microRNA26a, which constrained expression of the methyltransferase EZH2. EZH2 activated the Notch pathway by suppressing Notch repressors, Numb and Fbxw7, via H3K27me3, and consequently stimulated T cell polyfunctional cytokine expression and promoted their survival via Bcl-2 signaling. Moreover, human shRNA-knockdown-*EZH2*-deficient T cells elicited poor anti-tumor immunity. $EZH2^{+}CD8^{+}$ T cells were

Correspondence should be addressed to W.Z. (; Email: wzou@med.umich.edu) or G.W. (; Email: wangguobin1954@126.com). Weiping Zou, M.D., Ph.D. at the Department of Surgery, University of Michigan School of Medicine, 109 Zina Pitcher Place, Ann Arbor, MI, 48109. Guobin Wang, M.D., Ph.D. at the Union Hospital, Tongji Medical College, Huazhong University of Science and Technology, Wuhan, China.

[11]Ende Zhao and Tomasz Maj shared first authorship.

AUTHOR CONTRIBUTIONS E. Z, T.M, and I.K. designed and performed most of the experiments, interpreted the data and drafted the paper; W.L., K.W., L.Z., S.Wei, J.C., S.Wan, L.V., W.S. and I.S. performed experiments; Y.W., Y.L., S.V., A.M.C., T.H.W., V.E.M., J.K., H.W., Y. Z., Z.W., R.L. and G.W. provided reagents, or clinical specimens and clinopathological information and interpreted the data. W.Z., I.K. and/or G.W. supported, conceived of and supervised the research, designed experiments and wrote the paper.

COMPETING FINANCIAL INTERESTS The authors declare no competing financial interests.

associated with improved cancer patient survival. Together, the data unveil a novel metabolic target and mechanism of cancer immune evasion.

Keywords

microRNA; glycolysis; metabolism; memory T cell; EZH2; polyfunctionality; epigenetic; H3K27; Notch; Bcl and tumor immunity

Effector T cells, particularly polyfunctional effector T cells, are capable of producing multiple effector cytokines and cytotoxic proteases following activation, mediate potent protective immunity, and are associated with beneficial immune responses against viral infection[1–5]. Inadequate T cell activation might result in dysfunctional states of T cells, including anergy, exhaustion, and senescence[6–8]. It has been recently reported that a switch from oxidative phosphorylation to glycolysis is important for memory T cell activation and effector function[9,10]. Given that nutrients including glucose are poorly replenished in the tumor, it is reasonably assumed that T cell glycolytic metabolism has been altered in the tumor microenvironment[10]. However, if and how human primary tumor-associated glycolytic metabolism impacts on effector T cell phenotype, function, and the *in vivo* anti-tumor immunity and clinical outcome, remains to be defined in patients with cancer.

Enhancer of zeste homolog 2 (EZH2) is the catalytic subunit of polycomb-group family members with histone methyltransferase activity of trimethylating histone H3 on lysine 27 (H3K27me3)[11,12]. H3K27me3 is a repressive epigenetic mark and mediates transcriptional repression in cancer cells[12]. Recent studies suggest that EZH2 is involved in T_H1 and T_H2 differentiation in mice[13,14]. In the current study, we have found that human T cell EZH2 controls effector T cell polyfunctionality and survival. Interestingly, EZH2 is a central target and sensor of glycolytic metabolism in the tumor microenvironment. Furthermore, we have demonstrated that EZH2 expression in T cells is regulated by glycolytic metabolism via microRNAs and is functionally and clinically relevant in patients with ovarian cancer.

Results

EZH2$^+$ T cells are polyfunctional and apoptosis resistant

Immunohistochemistry analysis has demonstrated that memory T cell tumor infiltration is associated with improved cancer patient survival[15–17]. However, it is unknown which specific and functional T cell subset(s) truly mediates anti-tumor immunity *in vivo* and is associated with long-term patient survival. In the research of this functional T cell subset, we noticed that EZH2 has been recently reported to control both T_H1 and T_H2 cell differentiation from naïve T cells in mice[13,14]. We hypothesized that EZH2 might regulate the effector cytokine profile of memory T cells in humans and particularly in patients with cancer. To explore the link between EZH2 and T cell function, we examined EZH2$^+$ T cells in different human tissues, and analyzed their phenotype. Immunofluorescence staining revealed the existence of EZH2$^+$CD3$^+$ T cells in tonsil, spleen, and ulcerative colitic colon tissues (Supplementary Fig. 1a). Polychromatic flow cytometry analysis demonstrated that peripheral blood EZH2$^+$ T cells were confined to CD45RA$^-$CD62L$^-$CD45RO$^+$ memory

cells (Fig. 1a). Both $EZH2^+CD4^+$ and $EZH2^+CD8^+$ T cells did not express KLRG1, Tim-3 and CD57 (Fig. 1b). These markers are associated with T cell anergy and senescence[6,8]. Thus, $EZH2^+$ T cells are different from anergic and senescent memory T cells.

We further examined the effector cytokine profile and cytotoxic protease of $EZH2^+$ T cells (Supplementary Fig. 1b). $EZH2^+CD4^+$ T cells were enriched with cells expressing two and three effector cytokines of interleukin 2 (IL-2), interferon-γ (IFN-γ), and tumor necrosis factor (TNF, Fig. 1c,d). $EZH2^+CD8^+$ T cells were enriched with cells expressing double and triple effector molecules of IFN-γ, TNF and granzyme B (Fig. 1c,d). The data indicate that $EZH2^+$ T cells are enriched with multiple effector cytokine expressing (polyfunctional) T cells (Supplementary Fig. 1b).

Polychromatic flow cytometry analysis also detected $EZH2^+CD8^+$ T cells in the human ovarian cancer tissues. Again, ovarian cancer infiltrating $EZH2^+CD8^+$ T cells were phenotypically distinct from $KLRG1^+CD8^+$ T cells, $Tim\text{-}3^+CD8^+$ T cells and $CD57^+CD8^+$ T cells (Fig. 1e). Ovarian cancer-infiltrating $EZH2^+CD8^+$ T cells were also enriched with polyfunctional T cells (Fig. 1f). In addition to their polyfunctionality, TUNEL assay showed that there were less spontaneous apoptotic T cells in $EZH2^+$ T cells than $EZH2^-$ T cells in ovarian cancer tissues (Fig. 1g). Consistent with the anti-apoptotic role of Bcl-2 in human effector T cells[18,19], we observed that polyfunctional T cells and $EZH2^+$ T cells expressed high amounts of Bcl-2 (Fig. 1h,i). The data suggest that $EZH2^+$ T cells may have a survival advantage. To further support this possibility, we examined T cell survival in the presence of cisplatin, a first line chemotherapeutic agent for ovarian cancer. Cisplatin induced $CD8^+$ T cell apoptosis (Supplementary Fig. 1c) and increased the percentage of polyfunctional $CD8^+$ T cells. Cisplatin treatment did not change the absolute numbers of polyfunctional $CD8^+$ T cells (Fig. 1j). The data indicate that polyfunctional $CD8^+$ T cells were relatively resistant to cisplatin-induced apoptosis. Consistent with this observation, EZH2 expression was increased in $CD8^+$ T cells after cisplatin treatment (Supplementary Fig. 1d). Altogether, $EZH2^+CD8^+$ T cells were enriched with polyfunctional T cells (Fig. 1f) and experienced less spontaneous (Fig. 1g) and chemotherapy-induced (Fig. 1j) apoptosis compared to $EZH2^-$ T cells in the human ovarian cancer microenvironment. Thus, it is reasoned that $EZH2^+$ T cells may be functional effector T cells in the tumor microenvironment and mediate potent anti-tumor immunity. However, the ratios between $EZH2^+CD8^+$ effector T cells and dysfunctional T cells ($KLRG1^+$, $Tim\text{-}3^+$ or $CD57^+$) were lower in ovarian cancer compared to peripheral blood (Fig. 1k–m) and relatively “normal” ovary cysts (Fig. 1n–p). The imbalance between functional effector T cells and dysfunctional T cells suggests a relative loss of polyfunctional effector T cells in the cancer microenvironment.

EZH2 regulates effector T cell polyfunctionality and survival

Given that EZH2 expression coincided in polyfunctional and apoptotic resistant effector T cells, we hypothesized that EZH2 may functionally regulate T cell polyfunctional cytokine profile and survival. To test this hypothesis, we activated T cells with anti-CD3 and anti-CD28 antibodies. We observed increased expression of EZH2 protein and H3K27me3 upon T cell activation (Fig. 2a, Supplementary Fig. 2a). Interestingly, biochemical inhibition of EZH2 expression with DZNep[20] resulted in reduced double- and triple-positive $CD8^+$ T

cells for IFN-γ, TNF and granzyme B expression (Fig. 2b,c). As a confirmatory experiment, we genetically knocked down EZH2 expression with EZH2-specific short hairpin RNA (shEZH2). As expected, shEZH2 caused reduced expression of EZH2 and H3K27me3 and decreased polyfunctional $CD8^+$ T cells (Fig. 2d–f).

To test the effect of EZH2-associated H3K27me3 on T cell polyfunctionality, we employed EZH2-specific S-adenosylmethionine-competitive lead inhibitor compound GSK126 identified through high-throughput biochemical screen by GSK[21]. T cells treated with GSK126 showed complete loss of EZH2 associated H3K27me3 mark without any change in EZH2 protein abundance (Fig. 2g). GSK126 treatment inhibited polyfunctionality as shown by reduced double- and triple-positive $CD8^+$ T cells (Fig. 2h,i). The data indicate that EZH2 regulates T cell polyfunctionality via EZH2 associated H3K27me3.

As $EZH2^+$ T cells are more resistant to apoptosis, we questioned whether EZH2 is also involved in the control of effector T cell survival. In support of this possibility, flow cytometry analysis demonstrated that treatment with DZNep or GSK126 increased the percentage of Annexin V^+ T cells under TCR engagement (Fig. 2j). Similarly, shEZH2 viral transfection caused increased T cell apoptosis (Fig. 2j). In further support of the nature of EZH2-mediated anti-apoptosis, we observed that DZNep treatment reduced Bcl-2 mRNA and protein expression in T cells (Supplementary Fig. 2b, Fig. 2k). Inhibition of EZH2 promoted the expression of pro-apoptotic genes Bak, Bax and Bim in T cells (Supplementary Fig. 2c). T cells transfected with shEZH2 expressed less Bcl-2 (Fig. 2l). Furthermore, genetic knockdown of EZH2 reduced *BCL2* promoter activity (Fig. 2m). The data indicate that EZH2 may regulate Bcl-2 expression and consequently control effector T cell survival. Thus, EZH2 is a key regulatory gene controlling effector T cell polyfunctionality and survival.

EZH2 inhibits T cell Notch repressors

Next we explored how EZH2 regulates effector T cell polyfunctionality and survival. The Notch signaling pathway regulates effector T cell survival[19,22] and effector function including cytokine expression[23]. We hypothesized that EZH2 altered the Notch signaling pathway and in turn affected T cell cytokine profile and survival. As expected, when human T cells were activated, EZH2 and intracellular domain of Notch (NICD) were synchronically induced (Fig. 3a). Genetic silencing of EZH2 with shEZH2 decreased the amount of NICD (Fig. 3b). DZNep treatment suppressed Notch signaling activation as shown by reduced *HES1*, *HEY1*, and *HEY2* expression (Fig. 3c). Those data indicate that EZH2 may promote Notch signaling activation in T cells. EZH2 is one of the PcG family members with transcriptional repression function[12]. We hypothesized that EZH2 targeted and repressed Notch repressors and consequently activated Notch. Numb and Fbxw7 are two important Notch suppressors[24,25]. In support of our hypothesis, blockade of EZH2 expression led to elevated expression of *NUMB* and *FBXW7* (Fig. 3d). EZH2 exerts transcriptional repression through H3K27me3 (ref.[12]). ChIP assays revealed high occupancies of H3K27me3 in the proximal promoter areas of *NUMB* and *FBXW7*, whereas genetic knock-down of EZH2 abrogated these occupancies (Fig. 3e). The data suggests that EZH2 targets Notch repressors and promotes Notch activation, and may consequently regulate effector T cell

polyfunctionality and survival. In line with this, we observed that Notch inhibitors, N-[N-(3,5-Difluorophenacetyl)-L-alanyl]-S-phenylglycine t-butyl ester (DAPT) and gamma-secretase inhibitor I (GSI-I) suppressed double- and triple-positive $CD8^+$ T cells for IFN-γ, TNF, and granzyme B, and increased effector T cell apoptosis (Fig. 3f–h, Supplementary Fig. 3a). Furthermore, ectopic expression of the Notch active domain (Notch-IC) increased *BCL2* promoter activity (Supplementary Fig. 3b). The data suggests that EZH2 targets Notch repressors and promotes Notch activation, affects Bcl-2 activation and controls effector T cell polyfunctionality and survival.

Tumor impairs T cell function via glucose restriction

Polyfunctional T cells mediate potent anti-viral immunity[1–5]. Substantial studies focus on T cell exhaustion and senescence. However, it is poorly understood why there is a relative loss of $EZH2^+$ polyfunctional T cells in the cancer microenvironment. To address this question, we initially examined how polyfunctional T cells were regulated in the tumor microenvironment. A switch from oxidative phosphorylation to aerobic glycolysis is crucial for acquiring the effector functions by T cells[9,10]. We hypothesized that tumor reduced polyfunctional T cells via glucose restriction. To test this hypothesis, we cultured $CD8^+$ T cells with normal medium, tumor medium from primary ovarian cancer cells[26], normal medium with additional 2 mg/ml glucose supplementation, and tumor medium with additional 2 mg/ml glucose supplementation (Fig. 4a). We subsequently analyzed their ability to undergo a metabolic switch and its association with polyfunctional T cells. Tumor medium contained low concentrations of glucose (Fig. 4a). As expected, T cells cultured in normal medium efficiently responded to TCR engaged activation and increased extracellular acidification rate (ECAR). On the contrary, $CD8^+$ T cells cultured in tumor medium were poorly responsive to activation as demonstrated by reduced ECAR (Fig. 4b). Glucose supplementation partially rescued ECAR from T cells cultured with tumor medium, but had no effect on ECAR from T cells cultured with normal medium (Fig. 4a,b). We further evaluated the ratio between ECAR and oxygen consumption rate (OCR) in $CD8^+$ T cells conditioned with ovarian cancer medium. We observed a lower ECAR/OCR ratio in tumor conditioned T cells than controls (Fig. 4c). Accompanied with a reduced ECAR and ECAR/OCR ratio, co-culture with primary cancer cells resulted in lower numbers of polyfunctional $CD8^+$ T cells as shown by reduced double-positive and triple-positive $CD8^+$ T cells, and high frequencies of apoptotic $CD8^+$ T cells (Fig. 4d–f). Again, glucose supplementation reversed these effects (Fig. 4d–f). Similar results were obtained in polyfunctional $CD4^+$ T cells (Supplementary Fig. 4a,b). We further cultured $CD8^+$ T cells in normal medium containing low concentration of glucose (0–1 mg/ml), which was similar to that in tumor media. We found that low concentrations of glucose resulted in reduced double- or triple-positive polyfunctional $CD8^+$ T cells (Supplementary Fig. 4c) and a higher frequency of apoptosis (Supplementary Fig. 4d). We also examined the influence of glucose on the expression of B7-H1 (PD-L1) and B7-H4 in ovarian cancer cells. Glucose restriction or supplementation did not alter their expression (Supplementary Fig. 4e). Furthermore, the hexokinase inhibitor 2-deoxy-D-glucose (2-DG) treatment reduced the number of polyfunctional T cells and increased the percentage of apoptotic T cells (Fig. 4g,h, Supplementary Fig. 4f). Taken together, the data suggest that tumor impairs T cell glycolysis, inhibits their polyfunctionality and promotes their apoptosis.

Tumor controls T cell EZH2 via specific microRNAs

EZH2 regulates T cell polyfunctionality and survival. Tumor microenvironments impair T cell polyfunctionality and survival via glucose restriction. T cell activation induced EZH2 expression. We hypothesized that the tumor environment controls T cell EZH2 induction via glucose restriction and in turn, regulates T cell polyfunctionality and apoptosis. To test this hypothesis, we activated and cultured T cells in the presence of primary ovarian cancer supernatants, and examined EZH2 expression. We observed that tumors impaired EZH2 expression in both $CD4^+$ and $CD8^+$ T cells (Fig. 5a,b, Supplementary Fig. 5a). Interestingly, glucose supplementation rescued EZH2 expression (Fig. 5a,b, Supplementary Fig. 5a). Low concentrations of glucose in normal medium also caused reduced EZH2 expression (Supplementary Fig. 5b). The data suggest that tumor impaired T cell EZH2 expression via glucose restriction. In line with this possibility, we observed that 2-DG strongly inhibited EZH2 expression in both $CD4^+$ and $CD8^+$ T cells (Fig. 5c). Thus, tumor microenvironments reduce EZH2 expression via glucose metabolism impairment.

Next we examined how tumor cells impair T cell EZH2 expression. MicroRNA101[27] and microRNA26a[28] regulate EZH2 expression in tumor cells. In parallel to the increase in EZH2 expression, the abundance of microRNA101 and microRNA26a were rapidly reduced in the course of T cell activation, whereas many microRNAs including microRNA223, microRNA106b and microRNA181a were not changed (Fig. 5d,e, Supplementary Fig. 5c). In the presence of tumor cells, however, the expression of microRNA101 and microRNA26a remained high and additional glucose significantly reduced their expression (Fig. 5f,g). In line with this observation, abundant microRNA101 and microRNA26 was detected in T cells cultured in normal medium supplemented with limited glucose as compared to normal glucose concentrations (Supplementary Fig. 5d). This observation suggests that tumor may promote and sustain microRNA101 and microRNA26a expression in T cells via glucose restriction. In further support of this, 2-DG treatment prevented the loss of microRNA101 and microRNA26a in T cells activated with TCR engagement (Fig. 5d–g). As expected, transfection of T cells with microRNA101 and microRNA26a mimics led to the reduction of EZH2 expression, decreased polyfunctional T cells, and enhanced T cell apoptosis (Fig. 5g–j). Accordingly, the absolute numbers of viable T cells were reduced in cells transfected with microRNA101 and microRNA26a mimics (Supplementary Fig. 5e).

MicroRNA101[27] and microRNA26a[28] target EZH2 through specific 3′-UTR. To determine whether microRNA101 and microRNA26a may target other gene(s), and regulate T cell survival and polyfunctionality, we constructed a vector encoding EZH2 without 3′-UTR[27] and overexpressed this EZH2-expressing vector in T cells. As expected, microRNA101 and microRNA26a mimics had no effect on EZH2 expression in T cells with EZH2 overexpression (Supplementary Fig. 6a). MicroRNA101 and microRNA26a mimics inhibited *Bcl2* expression, *Hey1* expression and polyfunctional $CD8^+$ T cell formation in control T cells, but not in EZH2- overexpressing T cells (Supplementary Fig. 6b–d). Thus, we propose that cancer mediates effector T cell dysfunction by targeting microRNAs, EZH2 and the Notch repressor-signaling pathway via aerobic glycolysis restriction (Fig. 5k).

EZH2 affects tumor immunity and patient survival

EZH2 marks polyfunctional T cells and controls their survival. We wonder whether EZH2 can affect T cell-mediated anti-tumor immunity *in vivo*. To this end, we employed a mouse lung metastasis model with melanoma. Adoptively transferred tumor-specific T cells protected mice from lung metastasis (Fig. 6a). Pre-treatment of T cells with DZNep inhibited the expression of EZH2 and H3K27me3, and impaired the protective role of T cells as shown by increased tumor foci in the lung (Fig. 6a). Similarly, specific EZH2 knockdown in T cells increased lung metastasis as compared to scrambled control shRNA (Fig. 6b). We further examined the effects of EZH2 on T cell-mediated anti-tumor immunity in a humanized ovarian cancer model[19,29]. Human ovarian cancer specific T cells were treated with DZNep and were intravenously transfused into ovarian cancer-bearing mice as previously described[19]. We observed increased tumor growth in mice that received tumor-specific T cells pretreated with DZNep *in vitro* compared to the mice that received T cells without DZNep treatment (Fig. 6c). In support of this, EZH2 inhibition reduced T cell polyfunctionality. Thus, EZH2 controls polyfunctional T cell-mediated anti-tumor immunity *in vivo*.

Based on their surface phenotype, tumor infiltrating T cell subsets have been studied in human cancers[29,30]. Given the polyfunctional profile of $EZH2^+$ T cells, we hypothesized that tumor-infiltrating $EZH2^+CD8^+$ T cells positively impact cancer survival. To test this hypothesis, we quantified the frequencies of $EZH2^+CD8^+$ T cells via immunohistochemistry in 135 ovarian cancer tissues with available clinical and pathological information (Supplementary Table 1). Based on the median values of $CD8^+$ T cell numbers, $EZH2^+CD8^+$ T cell numbers, and the percentage of $EZH2^+CD8^+$ T cells in total $CD8^+$ T cells, we divided patients into “low” and “high” groups. Univariate analysis demonstrated no significant correlations between the number of $CD8^+$ T cells and overall patient survival (Fig. 6d, Supplementary Table 1), and between the number of $CD8^+$ T cells and disease-free interval (Fig. 6e and Supplementary Table 1). However, $EZH2^+CD8^+$ T cell numbers and the percentage of $EZH2^+CD8^+$ T cells highly correlated with improved overall survival and disease-free interval (Fig. 6f–i and Supplementary Table 1). Age, tumor stage, and debulking and grade were important prognostic factors for both overall and disease-free survival (Supplementary Table 1). After adjusting for these clinical prognostic factors as well as histology, $EZH2^+CD8^+$ T cell number and percentage remained significant predicators for overall survival and disease-free survival (Supplementary Tables 2–4).

To precisely estimate the performance of $CD8^+$ T cell numbers, $EZH2^+CD8^+$ T cell numbers, and the percentages of $EZH2^+CD8^+$ T cells for predicting survival, we used the time-dependent receiver operating characteristic (ROC) curve analysis[31]. The area under the ROC curve (AUC) is calculated to evaluate the predictive accuracy of each marker for estimating long-term (10-year) survival. AUC for $CD8^+$ T cell infiltration was significantly lower as compared to $EZH2^+CD8^+$ cells expressed in both number and percentage (Fig. 6j,k). This finding indicates that expression of EZH2 in $CD8^+$ T cells is a stronger predictor for cancer patient long-term overall survival and disease-free interval as compared to $CD8^+$ T cells (Fig. 6j,k). Moreover, the percentage of $EZH2^+CD8^+$ T cells was associated with significantly higher AUC as compared to that of $CD8^+$ T cell number and $EZH2^+CD8^+$ T

cell number for both overall survival and disease-free interval (Fig. 6j,k). Similar results were obtained for survival from 6 to 8 years. The data suggest that the fraction of $EZH2^+CD8^+$ T cells precisely predicts ovarian cancer patient outcome and particularly long-term survival. Altogether, our results demonstrate how EZH2 marks polyfunctional T cells and controls tumor immunity and impacts patient outcome.

Discussion

Effector memory T cells including polyfunctional T cells mediate potent protective immunity in viral infection[1–5]. Although T cell tumor infiltration is associated with improved patient survival[15–17], the nature of their effector function including survival and polyfunctionality remains poorly understood. Furthermore, memory T cell subsets are under active investigation in the context of immune vaccination, T cell therapy, and inhibitory check-point blockade therapy[6,19,32–36]. It has been proposed that memory T cell differentiation status, survival and stemness properties[19,34–37] and the subset of $CD27^+CD28^+$ T cells[37] may be crucial factors determining their anti-tumor potency[19,34–36,38]. However, which T cell subset truly mediates anti-tumor immunity *in vivo* in patients with cancer is not well defined. Understanding the features of the truly protective T cells in cancer patients will provide significant guidance for designing T cell therapies and evaluating therapeutic efficacy of immune vaccination and therapy. In the current work, we have phenotypically, functionally, and clinically demonstrated that $EZH2^+$ T cells mediate potent anti-tumor immunity in human cancer and are associated with long-term survival.

Epigenetic and chromatin remodeling may rapidly occur in activated memory T cells[9]. We found that 48 hours after TCR engagement, substantial EZH2 expression was induced in T cells. EZH2 expression highly coincides in polyfunctional memory T cells. Major transcriptional factors including T-bet, GATA-3, and RORγt control T_H1, T_H2, and T_H17 effector T cell subset differentiation and function. It is unknown whether polyfunctional T cells are controlled by a major transcription factor. Although EZH2 is not known as a transcription factor, we demonstrate that EZH2 is involved in defining the survival and polyfunctional cytokine profile of effector T cells. In order to further study the mechanism by which EZH2 controls effector T cell survival and polyfunctionality, we have shown that EZH2 directly binds to the promoter areas of Notch repressors, *NUMB* and *FBXW7*, and represses their transcription via H3K27me3, and subsequently causes Notch activation, which results in anti-apoptotic gene activation and effector cytokine expression. Thus, EZH2 targets the Notch signaling pathway to regulate effector T cell polyfunctionality and survival.

Given the functional and mechanistic importance of EZH2 in polyfunctional T cells in cancer, it is essential to dissect how T cell EZH2 is controlled in the tumor microenvironment, a hypoglycemic environment due to the Warburg effect. Interestingly, we have found that primary ovarian cancer cells reduce EZH2 expression and limit polyfunctional cytokine expression and survival of effector T cells, which can subsequently be rescued by glucose supplementation and mimicked by 2-DG treatment. This observation suggests that T cell EZH2 is controlled by glycolytic metabolism in the cancer environment. In line with our observations, recent studies have demonstrated that glycolytic switch

regulates memory T cell activation, proliferation, and IFN-γ expression in mouse models[9,10,39]. Further mechanistic studies have shown that tumor cells sustain high expression of microRNA26a and microRNA101 in effector T cells. Consequently, these microRNAs lessen EZH2 expression and cause effector T cell dysfunction. Thus, our data reveal a novel metabolic target and mechanism of cancer immune evasion: cancer restricts T cell EZH2 expression through limiting their aerobic glycolysis and consequently weakens T cell-mediated anti-tumor immunity.

Our studies have important clinical application. The ability of persistence and survival is critical for tumor-associated antigen (TAA)-specific T cells to exert their anti-tumor effects[34]. T_H17 cells have survival advantage with stem cell properties[19,36,38,40]. In line with this notion, now we have found that polyfunctional T cells express EZH2 and have survival advantages in the cancer microenvironment. It is logical that the fraction of $EZH2^+CD8^+$ T cells significantly and precisely predicts patient outcome. Our work indicates that polyfunctional $CD8^+$ T cells are a precise prognostic factor for long-term cancer survival. Furthermore, $EZH2^+CD8^+$ T cells may be a valuable marker for testing and screening clinical efficacy of immune therapy and vaccination. It is reasonable to assume that enhancing and/or maintaining EZH2 expression in T cells may be therapeutically meaningful in treating patients with cancer. On the other hand, EZH2 is highly expressed in various human cancer cells[27,41]. Systemic epigenetic therapy including EZH2 blockade has been considered a powerful regimen to treating patients with cancer[42,43]. Given the current overwhelming interests in epigenetic therapy, our data suggest that the potential effect of systemic epigenetic manipulation on T cell effector function should be taken into consideration. T cells and tumor cells may be differentially sensitive to epigenetic manipulation. A tumor specific targeting approach or the use of minimal effective dosage should be a wise option to clinically explore epigenetic therapy. Furthermore, the combination of epigenetic therapy and immunotherapy may be sequentially implicated to enhance the therapeutic efficacy and to minimize the potential side effect of certain epigenetic modifier(s). In the context of autoimmunity, T cells express high amounts of EZH2 in the microenvironment of ulcerative colitis, and it is assumed that inhibition of EZH2 expression or EZH2-associated signaling in T cells might be therapeutically beneficial.

In summary, we have demonstrated that the $EZH2^+CD8^+$ T cell is a functional effector T cell subset in human cancer, that EZH2 marks and controls effector T cell polyfunctionality and survival through microRNAs-EZH2-Notch signaling pathway, and that this pathway is regulated by glucose metabolism in the tumor microenvironment. Manipulation of this pathway may be useful in treating patients with cancer.

Methods

Ovarian cancer patients and human tissues

Patients diagnosed with ovarian cancer were recruited for this study. We collected 135 formalin-fixed, paraffin-embedded ovarian tumor tissue blocks, 20 snap-frozen ovarian tumor tissues, and 37 fresh ovarian cancer tissues and 11 ovary cysts for this study, as previously described[29, 44–46]. After pathological review, a tissue microarray (TMA) was

constructed from the most representative area of paraffin-embedded ovarian tumor tissue. For each tumor, a minimum of two representative tumor areas were selected from a hematoxylin- and eosin-stained section of a donor block. Core cylinders (1 mm) were punched from each of these areas and deposited into a recipient paraffin block. Consecutive 6 μm-thick TMA sections were cut and placed on charged Poly-L-Lysine-coated slides for immunohistochemistry analyses. Donors were given written, informed consent. In addition to ovarian cancer tissues, human spleen, tonsil, and ulcerative colitic colon tissues were obtained from the tissue procurement core at the University of Michigan Hospital. The study was approved by the local Institutional Review Boards.

Animal studies

B16 melanoma lung metastasis model. We intravenously injected B16 melanoma cells into C57BL/6 mice and established lung metastasis. Melanoma-specific T cells were generated as previously described. Melanoma-specific T cells were activated in the presence or absence of 1 μM DZNep for 2 days, or melanoma-specific T cells were transfected with lentivirus vectors encoding either shEZH2 or scramble and activated for 2 days, then washed and expanded in 80 IU/ml IL-2 for 3 days and intravenously transfused into mice bearing melanoma lung metastasis. After 7 days, the mice were sacrificed. Lung metastatic foci were recorded.

Human ovarian cancer chimeric model

Primary ovarian cancer cells were isolated from ovarian cancer ascites fluid and ovarian cancer tissues[44,47]. Ovarian cancers were subcutaneously established in female NOD/Shi-scid/IL-2Rcnull (NSG) mice (6 ~ 8 weeks old; Jackson Laboratory)[44,47]. Autologous tumor-specific T cells were generated as previously described[19]. Tumor specific T cells were treated with 1 μM DZNep for 3 days and washed, then intravenously transfused into mice bearing autologous ovarian cancer. Tumor volume was measured every 4 days. All animal studies were conducted under the approval of the University of Michigan Committee on Use and Care of Animals.

Manipulation of EZH2 and Notch signaling pathways

Short hairpin RNA with an EZH2-specific (shEZH2) or scramble sequence was packed into a lentivirus packaging construct and transfected into HEK293T cells with lipofectamine 2000 (Invitrogen). EZH2 expression was genetically blocked in human primary memory T cells with lentivirus encoding shEZH2 or scramble. 2–5 μM 3-deazaneplanocin A·HCl (DZNep) and 10 μM GSK126 (Glixx Laboratories) were utilized to biochemically block EZH2 and EZH2 methyltransferase activity, respectively. The vectors encoding an active domain of Notch (Notch-IC) or a negative domain were used to genetically activate or block Notch signaling, respectively[19,48]. The Notch signaling pathway was biochemically manipulated with two Notch inhibitors: DAPT (Santa Cruz Biotech) and GSI-I (Calbiochem).

Fluorescence activated cell sorting and flow cytometry analysis

Cells were first stained extracellularly with specific antibodies against human CD3 (clone HIT3a), CD4 (clone RPA-T4), CD8 (clone HIT8a), CD45RA (clone HI100), CD45RO (clone UCHL1), CD57 (clone NK-1), CD62L (clone DREG56) (BD Bioscience), KLRG-1 (clone 13F12F2, eBioscience) and Tim-3 (clone #344823) (R&D), were fixed and permeabilized with Fixation/Permeabilization solution (eBioscience), and finally were stained intracellularly with anti-tumor necrosis factor (TNF, clone Mab11), anti-IFN-γ (clone B27), anti-granzyme B (clone GB11), anti-Bcl-2 (clone Bcl-2/100), and anti-EZH2 (clone 11/EZH2) (BD Biosciences). Samples were acquired on a flow cytometry analyzer (LSR II; BD Biosciences) and data were analyzed with DIVA software (BD Biosciences). For lentivirus-infected cells, GFP^+ cells were sorted with a FACSAria cell sorter (BD Biosciences).

Cell apoptosis detection

Cell apoptosis was measured with the Annexin V apoptosis detection kit (BD Bioscience). 2–5 μM DZNep and 10 μM GSK126 (Glixx Laboratories) were added into the cell culture as indicated.

Metabolic assay

T cell metabolism was measured in a Seahorse XF^e24 analyzer on V7-PET XF24 cell culture microplates (Seahorse Bioscience). One day before the assay, the plate was coated with Cell-Tak reagent (BD Biosciences) accordingly to the manufacturer's instruction. Next, 5×10^5 T cells were seeded into the wells and gently centrifuged twice for uniform distribution in the well. After 30 min of incubation, the assay medium was added to the cells and the experiment was performed. Normal medium was RPMI1640 containing 2 mg/ml glucose without sodium bicarbonate and fetal calf serum adjusted to pH 7.4. Normal medium and ovarian cancer culture medium were used in the assay. Different metabolic modifiers were added as indicated. Before seeding on the test plate, the cells were washed three times in assay medium to buffering compounds. T cells were stimulated with 2.5 μg/ml anti-CD3 (clone UCHT1) and 1.25 μg/ml anti-CD28 (clone CD28.2) with or without 2-deoxy-D-glucose (2-DG, 50 mg/ml) (Sigma-Aldrich).

T cell culture

Human peripheral blood T cell subsets (10^6/ml) were activated with anti-CD3 (clone UCHT1, 2.5 μg/ml) and anti-CD28 (clone CD28.2, 1.25 μg/ml) antibodies (BD Bioscience) for 3–5 days, as indicated in the figure legends. To obtain tumor medium, primary ovarian cancer cells were cultured for 3 days, and subsequently were frozen and thawed 5 times along with the culture medium. The cancer cell culture supernatant was obtained through centrifugation (20,000*g*, 1 h, 4°C), and used to culture T cells with or without glucose (2 mg/ml, Sigma Aldrich) supplementation for 16–24 h. To obtain normal medium containing different concentrations of glucose, normal medium without glucose (Invitrogen) was supplemented with 1 or 5 mg/ml glucose. Chemical inhibitors of metabolic pathways, Notch signaling or EZH2 were added as indicated in figure legends. Total numbers of viable cells at the endpoint of experiments were $1–2 \times 10^6$ cells.

Immunoblot

Immunoblotting was performed using the following primary antibodies EZH2 (1:1000, 612667, BD Bioscience), H3K27me3 (1:1000, 07–449, Millipore), H3 (1:2000, 4499, Cell Signaling), NICD (1:1000, ab52301, Abcam), Bcl-2 (1:1000, 551107, BD Bioscience), and β-actin (1:5000, A5441, Sigma). Signals were detected by ECL reagent (GE Healthcare).

Quantitative real-time PCR

Total RNA was isolated with Trizol Reagent (Invitrogen). Quantitative real-time PCR was carried out to quantify cell cycling associated genes, Notch signaling genes, and apoptosis associated genes[19] (Supplementary Table 5).

MicroRNA detection and manipulation

MicroRNAs were analyzed with microRNA TaqMan assays (Life Technologies) accordingly to the manufacturer's instruction. To examine the roles of microRNAs, we transfected T cells with specific microRNA mimics or irrelevant oligonucleotide controls on day 2 using human nucleofection kit (Lonza). The cells were analyzed on day 3.

EZH2 overexpression

T cells were transfected with EZH2-pCMV plasmid[27,41] before activation with human nucleofection kit (Lonza).

BCL2 promoter assay

The human *BCL2* promoter sequence (−850 to +134, TSS as +1) was initially linked to GFP. HEK293T cells were transfected with viral vector encoding the human *BCL2* promoter in conjunction with vector controls or vector containing cDNA encoding shEZH2, Notch-IC, and Notch-DN[48]. The promoter activity was measured by the green fluorescence intensity of transfected cells. Data were shown as the relative intensities. The intensity of control-GFP reporter is defined as 100.

Chromatin immunoprecipitation (ChIP)

ChIP was performed as previously described[26,49]. Briefly, nuclear extracts were prepared from primary human cells. Mouse anti-human H3K27me3 (ab6002, Abcam) and normal IgG (sc-2027, Santa Cruz) antibodies were used for immunoprecipitation. ChIP primers (Supplementary Table 5) were designed to detect promoter fragments near transcription start sites on *NUMB* and *FBXW7* genes.

Immunofluorescence and immunohistochemistry staining

We performed immunofluorescence staining in frozen tissue sections. The primary antibodies were mouse anti-human EZH2 (1:100, 612667, IgG1, BD Bioscience), rabbit anti-human CD3 (1:100, A0452, IgG, Dako), and TUNEL (S7165, Millipore). The secondary antibodies were goat anti-mouse IgG1 conjugated with Alexa Fluor 488 and goat anti-rabbit IgG conjugated with Alexa Fluor 568. The stained tissue sections were analyzed under a fluorescent microscope. Immunohistochemistry staining was performed in paraffin-fixed ovarian cancer tissues (Dako EnVision Double stain System, Dako). Paraffin-

embedded TMA sections were deparaffinized and stained with rabbit anti-human EZH2 (1:200, 187395, Invitrogen) and followed by Polymer-HRP and DAB Chromogen treatment. TMA sections were subsequently stained with mouse anti-human CD8 (1:50, M7103, Dako), followed by treatment with Rabbit-Mouse LINK, Polymer-AP, Permanent Red Chromogen and hematoxylin counterstaining. The TMA cores were quantified and analyzed for expression of $EZH2^+$ and $CD8^+$ T cells with an Aperio imaging system (Genetix). The specimens were digitalized with an automated platform (Aperio Technologies) and ScanScope XT and Spectrum Plus using TMA software version 9.1 scanning system. Cores were scored in high resolution at 40X magnification. Tissue sections were scored manually on a computer screen, and a mean score for duplicate cores from each individual was calculated. Any discrepancies were resolved by subsequent consultation with diagnostic pathologists. CD8 was localized in the cell membrane and cytoplasm and EZH2 was localized in the nuclei. CD8 and EZH2 were scored quantitatively (the numbers of positive cells). The tissues were divided into high and low $CD8^+$ T cells (>7, <7), $EZH2^+CD8^+$ T cells (>2, <2), or the percentage (>22%, <22%) of $EZH2^+CD8^+$ T cells in $CD8^+$ T cells based on their median values per core (Supplementary Tables 1–4). Staining with isotype antibody was used as negative control.

Statistical analysis

Wilcoxon rank-sum tests were used to compare two independent groups, and for paired groups, Wilcoxon signed rank tests were used for the comparison. Correlation coefficients (Spearman correlation, denoted by r, for ordinal data and Pearson correlation, denoted by r, for continuous data), together with a P-value (null hypothesis is that r is in fact zero), were computed to measure the degree of association between biomarkers. Overall patient survival was defined from date of diagnosis to disease related death. Disease-free interval was defined from date of diagnosis to disease progression or disease related death. Data were censored at the last follow-up for patients who were disease-free or alive at the time of analysis. Survival functions were estimated by Kaplan-Meier methods. Cox's proportional hazards regression was performed to model survival as a function of the levels of $CD8^+$ T cells, $EZH2^+CD8^+$ T cells or the percentage of $EZH2^+CD8^+$ T cells in $CD8^+$ T cells (all classified as low and high based on the median value), after adjusting for age, stage, histology, and debulking. We assessed the adequacy of the Cox regression model Graphical and numerical methods as described[26,49,50]. To estimate the performance of the levels of $CD8^+$ T cells, $EZH2^+CD8^+$ T cells, and the percentage of $EZH2^+CD8^+$ T cells for predicting patient survival, we used the time-dependent receiver operating characteristic (ROC) curve analysis [31]. The area under the ROC curve (AUC) is calculated to evaluate each marker's predictive accuracy. We used this analysis to evaluate and compare the predictive accuracy of the levels of $CD8^+$ T cells, $EZH2^+CD8^+$ T cells, and the percentage of $EZH2^+CD8^+$ T cells for long-term survivals. All analyses were done using SAS 9.3 software. $P < 0.05$ considered as significant.

Supplementary Material

Refer to Web version on PubMed Central for supplementary material.

ACKNOWLEGDMENTS

This work is supported (in part) by the National Institutes of Health (NIH) grants (CA123088; CA099985; CA156685; CA171306; 5P30CA46592), the Chinese Ministry of Science and Technology (973 program, 2015CB554000), the Wuhan Union Hospital Research Fund, the Intramural Research Program of the NIH, National Cancer Institute, the Ovarian Cancer Research Fund, and Marsha Rivkin Center for Ovarian Cancer Research. We would like to thank D. Postiff, M. Vinco, R. Craig, and J. Barikdar in the tissue procurement core at the University of Michigan, and Gang Lv, Weihong Dong and Lei Li at the Union Hospital (Wuhan, China) for their assistance. We are grateful for R. Zhang for providing shEZH2 plasmids and P. King for valuable discussion. We particularly appreciate the generous support from Barbara and Don Leclair.

References

1. Ladell K, et al. A molecular basis for the control of preimmune escape variants by HIV–specific CD8+ T cells. Immunity. 2013; 38:425–436. [PubMed: 23521884]
2. Almeida JR, et al. Superior control of HIV–1 replication by CD8+ T cells is reflected by their avidity, polyfunctionality, and clonal turnover. J. Exp. Med. 2007; 204:2473–2485. [PubMed: 17893201]
3. Harari A, et al. An HIV–1 clade C DNA prime, NYVAC boost vaccine regimen induces reliable, polyfunctional, and long–lasting T cell responses. J. Exp. Med. 2008; 205:63–77. [PubMed: 18195071]
4. Gaucher D, et al. Yellow fever vaccine induces integrated multilineage and polyfunctional immune responses. J. Exp. Med. 2008; 205:3119–3131. [PubMed: 19047440]
5. Precopio ML, et al. Immunization with vaccinia virus induces polyfunctional and phenotypically distinctive CD8(+) T cell responses. J. Exp. Med. 2007; 204:1405–1416. [PubMed: 17535971]
6. Wherry EJ. T cell exhaustion. Nat. Immunol. 2011; 12:492–499. [PubMed: 21739672]
7. Zheng Y, Zha Y, Driessens G, Locke F, Gajewski TF. Transcriptional regulator early growth response gene 2 (Egr2) is required for T cell anergy in vitro and in vivo. J. Exp. Med. 2012; 209:2157–63. [PubMed: 23129747]
8. Crespo J, Sun H, Welling TH, Tian Z, Zou W. T cell anergy, exhaustion, senescence, and stemness in the tumor microenvironment. Curr. Opin. Immunol. 2013; 25:214–221. [PubMed: 23298609]
9. Gubser PM, et al. Rapid effector function of memory CD8+ T cells requires an immediate-early glycolytic switch. Nat. Immunol. 2013; 14:1064–1072. [PubMed: 23955661]
10. Chang CH, et al. Posttranscriptional control of T cell effector function by aerobic glycolysis. Cell. 2013; 153:1239–1251. [PubMed: 23746840]
11. Vire E, et al. The Polycomb group protein EZH2 directly controls DNA methylation. Nature. 2006; 439:871–874. [PubMed: 16357870]
12. Cao R, et al. Role of histone H3 lysine 27 methylation in Polycomb-group silencing. Science. 2002; 298:1039–1043. [PubMed: 12351676]
13. Tumes DJ, et al. The polycomb protein Ezh2 regulates differentiation and plasticity of CD4+ T helper type 1 and type 2 cells. Immunity. 2013; 39:819–832. [PubMed: 24238339]
14. Tong Q, et al. Ezh2 regulates transcriptional and posttranslational expression of T-bet and promotes Th1 cell responses mediating aplastic anemia in mice. J. Immunol. 2014; 192:5012–5022. [PubMed: 24760151]
15. Pages F, et al. Effector memory T cells, early metastasis, and survival in colorectal cancer. N. Engl. J. Med. 2005; 353:2654–2666. [PubMed: 16371631]
16. Zhang L, et al. Intratumoral T cells, recurrence, and survival in epithelial ovarian cancer. N. Engl. J. Med. 2003; 348:203–213. [PubMed: 12529460]
17. Kryczek I, et al. Phenotype, distribution, generation, and functional and clinical relevance of Th17 cells in the human tumor environments. Blood. 2009; 114:1141–1149. [PubMed: 19470694]
18. Marrack P, Kappler J. Control of T cell viability. Annu. Rev. Immunol. 2004; 22:765–787. [PubMed: 15032596]
19. Kryczek I, et al. Human TH17 Cells Are Long–Lived Effector Memory Cells. Sci. Transl. Med. 2011; 3:104ra100.

20. Miranda TB, et al. DZNep is a global histone methylation inhibitor that reactivates developmental genes not silenced by DNA methylation. Mol. Cancer Ther. 2009; 8:1579–1588. [PubMed: 19509260]
21. McCabe MT, et al. EZH2 inhibition as a therapeutic strategy for lymphoma with EZH2–activating mutations. Nature. 2012; 492:108–112. [PubMed: 23051747]
22. Ciofani M, Zuniga–Pflucker JC. Notch promotes survival of pre–T cells at the beta–selection checkpoint by regulating cellular metabolism. Nat. Immunol. 2005; 6:881–888. [PubMed: 16056227]
23. Amsen D, et al. Instruction of distinct CD4 T helper cell fates by different notch ligands on antigen–presenting cells. Cell. 2004; 117:515–526. [PubMed: 15137944]
24. Wirtz–Peitz F, Nishimura T, Knoblich JA. Linking cell cycle to asymmetric division: Aurora–A phosphorylates the Par complex to regulate Numb localization. Cell. 2008; 135:161–173. [PubMed: 18854163]
25. Oberg C, et al. The Notch intracellular domain is ubiquitinated and negatively regulated by the mammalian Sel–10 homolog. J. Biol. Chem. 2001; 276:35847–35853. [PubMed: 11461910]
26. Cui TX, et al. Myeloid-derived suppressor cells enhance stemness of cancer cells by inducing microRNA101 and suppressing the corepressor CtBP2. Immunity. 2013; 39:611–621. [PubMed: 24012420]
27. Varambally S, et al. Genomic loss of microRNA–101 leads to overexpression of histone methyltransferase EZH2 in cancer. Science. 2008; 322:1695–1699. [PubMed: 19008416]
28. Sander S, et al. MYC stimulates EZH2 expression by repression of its negative regulator miR-26a. Blood. 2008; 112:4202–4212. [PubMed: 18713946]
29. Curiel TJ, et al. Specific recruitment of regulatory T cells in ovarian carcinoma fosters immune privilege and predicts reduced survival. Nat. Med. 2004; 10:942–949. [PubMed: 15322536]
30. Galon J, et al. Type, density, and location of immune cells within human colorectal tumors predict clinical outcome. Science. 2006; 313:1960–1964. [PubMed: 17008531]
31. Heagerty PJ, Lumley T, Pepe MS. Time–dependent ROC curves for censored survival data and a diagnostic marker. Biometrics. 2000; 56:337–344. [PubMed: 10877287]
32. Scholler J, et al. Decade–long safety and function of retroviral–modified chimeric antigen receptor T cells. Sci. Transl. Med. 2012; 4:132ra153.
33. Ahmed R, Bevan MJ, Reiner SL, Fearon DT. The precursors of memory: models and controversies. Nat. Rev. Immunol. 2009; 9:662–668. [PubMed: 19680250]
34. Rosenberg SA, Restifo NP, Yang JC, Morgan RA, Dudley ME. Adoptive cell transfer: a clinical path to effective cancer immunotherapy. Nat. Rev. Cancer. 2008; 8:299–308. [PubMed: 18354418]
35. Gattinoni L, et al. A human memory T cell subset with stem cell–like properties. Nat. Med. 2011; 17:1290–1297. [PubMed: 21926977]
36. Zou W, Restifo NP. TH17 cells in tumour immunity and immunotherapy. Nat. Rev. Immunol. 2010; 10:248–256. [PubMed: 20336152]
37. Powell DJ Jr. Dudley ME, Robbins PF, Rosenberg SA. Transition of late-stage effector T cells to CD27+ CD28+ tumor-reactive effector memory T cells in humans after adoptive cell transfer therapy. Blood. 2005; 105:241–250. [PubMed: 15345595]
38. Wei S, Zhao E, Kryczek I, Zou W. Th17 cells have stem cell-like features and promote long-term tumor immunity. OncoImmunology. 2012; 1:516–519. [PubMed: 22754771]
39. Yang K, et al. T cell exit from quiescence and differentiation into Th2 cells depend on Raptor-mTORC1-mediated metabolic reprogramming. Immunity. 2013; 39:1043–1056. [PubMed: 24315998]
40. Muranski P, et al. Th17 cells are long lived and retain a stem cell–like molecular signature. Immunity. 2011; 35:972–985. [PubMed: 22177921]
41. Varambally S, et al. The polycomb group protein EZH2 is involved in progression of prostate cancer. Nature. 2002; 419:624–629. [PubMed: 12374981]
42. Tan J, et al. Pharmacologic disruption of Polycomb–repressive complex 2–mediated gene repression selectively induces apoptosis in cancer cells. Genes Dev. 2007; 21:1050–1063. [PubMed: 17437993]

43. Fiskus W, et al. Combined epigenetic therapy with the histone methyltransferase EZH2 inhibitor 3–deazaneplanocin A and the histone deacetylase inhibitor panobinostat against human AML cells. Blood. 2009; 114:2733–2743. [PubMed: 19638619]
44. Kryczek I, et al. B7–H4 expression identifies a novel suppressive macrophage population in human ovarian carcinoma. J. Exp. Med. 2006; 203:871–881. [PubMed: 16606666]
45. Curiel TJ, et al. Blockade of B7–H1 improves myeloid dendritic cell–mediated antitumor immunity. Nat. Med. 2003; 9:562–567. [PubMed: 12704383]
46. Zou W, et al. Stromal–derived factor–1 in human tumors recruits and alters the function of plasmacytoid precursor dendritic cells. Nat. Med. 2001; 7:1339–1346. [PubMed: 11726975]
47. Kryczek I, et al. Expression of aldehyde dehydrogenase and CD133 defines ovarian cancer stem cells. Int. J. Cancer. 2012; 130:29–39. [PubMed: 21480217]
48. Yamamoto N, et al. Role of Deltex–1 as a transcriptional regulator downstream of the Notch receptor. J. Biol. Chem. 2001; 276:45031–45040. [PubMed: 11564735]
49. Kryczek I, et al. IL–22CD4 T Cells Promote Colorectal Cancer Stemness via STAT3 Transcription Factor Activation and Induction of the Methyltransferase DOT1L. Immunity. 2014; 40:772–784. [PubMed: 24816405]
50. Lin DY, Wei LJ, Ying Z. Checking the Cox model with cumulative sums of martingale–based residuals. Biometrika. 1993; 80:557–572.

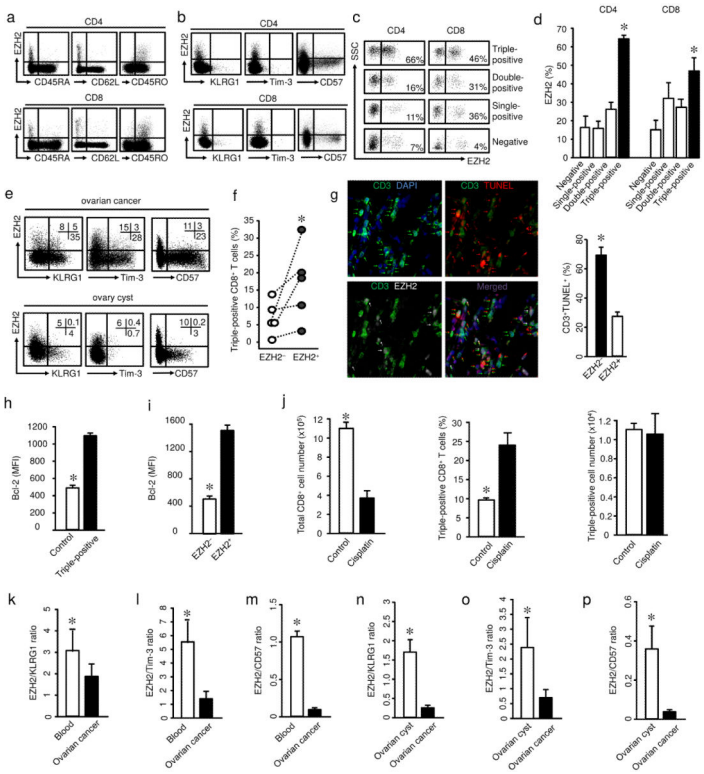

Fig. 1. EZH2$^+$ T cells endow polyfunctional and apoptosis resistant features

(**a,b**) Phenotype of EZH2$^+$ T cells. Peripheral blood mononuclear cells from healthy donors were stained with antibodies against EZH2, CD45RA, CD62L, CD45RO, KLRG1, Tim-3, CD57 and T cell markers, and analyzed with LSR II. One representative of 8 donors is shown.

(**c,d**) EZH2 and polyfunctional T cells in blood. Intracellular staining was performed in peripheral blood mononuclear cells for IFN-γ, TNF, and granzyme B. EZH2 expression was analyzed in CD4$^+$ T cells expressing single, double, triple, or no markers for IL-2, IFN-γ, and TNF, or CD8$^+$ T cells expressing single, double, triple or no markers for IFN-γ, TNF, and granzyme B. Results are shown as one of 6 flow cytometry dot plots (**c**) and the mean percentage ± SEM (**d**). Wilcoxon rank-sum test, *P <0.05.

(**e**) EZH2$^+$ T cells in ovarian cancer. Single cells were made from ovarian cancer tissues and were stained for T cell markers, KLRG1, Tim-3, CD57 and EZH2. CD8$^+$ T cells were analyzed by flow cytometry. Numbers in the quadrants are percentage of the cells in CD45$^+$CD3$^+$CD8$^+$ gate. One representative donor of 20 is shown.

(**f**) EZH2 and polyfunctional T cells in ovarian cancer. Intracellular staining was performed in single cells made from ovarian cancer tissues for T cell markers, IFN-γ, TNF, granzyme B, and EZH2. IFN-γ, TNF, and granzyme B triple positive (polyfunctional) CD8$^+$ T cells were analyzed on the basis of EZH2 expression. N = 5, Wilcoxon rank-sum test, *P <0.01.

(**g**) Relationship between EZH2 expression and T cell apoptosis in ovarian cancer. Frozen ovarian cancer tissues were stained with anti-CD3 (green), anti-EZH2 (white), TUNEL (red), and DAPI (blue). TUNEL$^+$CD3$^+$EZH2$^+$ T cells (White) are marked with white arrows. The percentage of TUNEL$^+$CD3$^+$ T cells (mean ± SEM) was determined in EZH2$^+$ and EZH2$^-$ T cells. N = 10, Wilcoxon rank-sum test, *P < 0.05.

(**h**) Expression of Bcl-2 in polyfunctional T cells. $CD8^+$ T cells were stimulated with anti-CD3 and anti-CD28 for 2 days. Expression of IFN-γ, TNF, granzyme B, and Bcl-2 was analyzed by flow cytometry. Results are shown as the mean fluorescent intensity (MFI) of Bcl-2 expression (mean ± SD) in polyfunctional (triple positive) $CD8^+$ T cells. N = 6, Wilcoxon rank-sum test, *P <0.05.

(**i**) Expression of Bcl-2 in $EZH2^+CD8^+$ T cells. $CD8^+$ T cells were stimulated with anti-CD3 and anti-CD28 for 2 days. Expression of EZH2 and Bcl-2 was analyzed by flow cytometry. Results are shown as the MFI of Bcl-2 expression (mean ± SD) in $EZH2^+CD8^+$ T cells. N = 6, Wilcoxon rank-sum test, *P <0.05.

(**j**) Effects of cisplatin on polyfunctional T cells. $CD8^+$ T cells were stimulated with anti-CD3 and anti-CD28 for 5 days. Cisplatin was added in culture on day 4. Cells were stained for polyfunctional phenotype (IFN-γ, TNF, and granzyme B). Total T cell number, the percentage and absolute numbers of triple-positive $CD8^+$ T cells were shown. N = 4, Wilcoxon rank-sum test, *P < 0.05.

(**k–m**) Ratios of EZH2/KLRG1 (k), EZH2/Tim-3 (l), and EZH2/CD57 (m) in ovarian cancer infiltrating T cells and peripheral blood T cells. The levels of KLRG1, Tim-3, and EZH2 expressing $CD8^+$ T cells were analyzed by flow cytometry. Results are shown as mean ± SEM. N = 30, Mann-Whitney U-test, *P < 0.05.

(**n–p**) Ratios of EZH2/KLRG1 (n), EZH2/Tim-3 (o), and EZH2/CD57 (p) in ovarian cancer infiltrating T cells and T cells in normal ovary cysts. $CD8^+$ T cells were analyzed by flow cytometry, data are shown as mean ± SEM. Ovary cyst tissues: N=11, cancer samples: N=7, Mann-Whitney U-test, *P < 0.05.

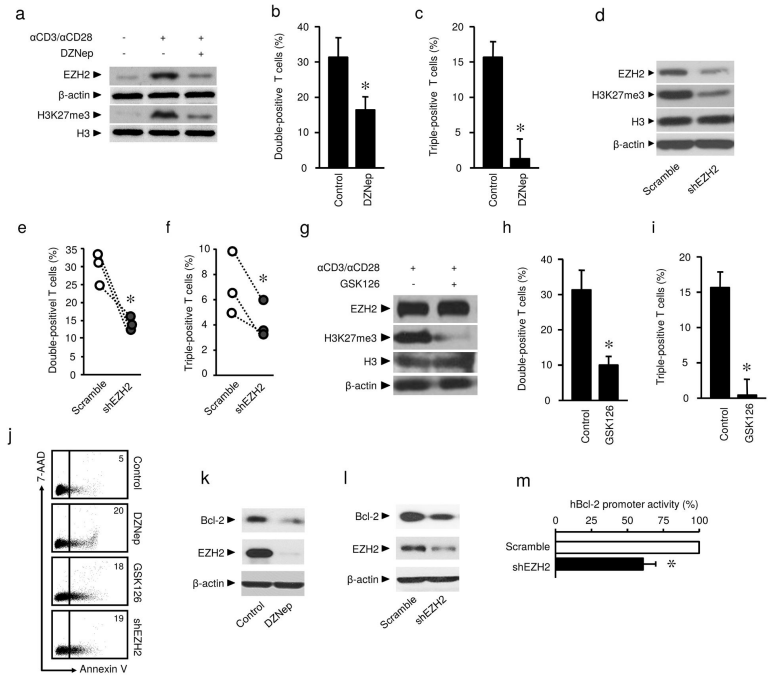

Fig. 2. EZH2 regulates effector T cell polyfunctionality and survival

(**a**) Effects of DZNep on EZH2 and H3K27me3 expression in T cells. T cells were stimulated with anti-CD3 and anti-CD28 antibodies for 3 days in the absence or presence of 5 μM DZNep. The expression of EZH2, H3K27me3, H3, and β-actin was measured with immunoblotting. One representative experiment of 4 is shown.

(**b,c**) Effects of DZNep on polyfunctionality of $CD8^+$ T cells. $CD8^+$ T cells were activated with anti-CD3 and anti-CD28 antibodies for 3 days in the absence or presence of 5 μM DZNep. Expression of IFN-γ, TNF, and granzyme B was analyzed by flow cytometry. The percentage of double (**b**) and triple-positive (**c**) cells is shown. Data presented as mean ± SEM, N=5, Wilcoxon rank-sum test, *P < 0.05.

(**d–f**) Effects of shEZH2 on EZH2 and H3K27me3 expression and polyfunctionality in $CD8^+$ T cells. T cells transfected with shEZH2 or scramble vectors were activated for 3 days. The expression of EZH2 and H3K27me3 was measured with immunoblotting (**d**). Expression of IFN-γ, TNF, and granzyme B was analyzed by flow cytometry. The percentage of double (**e**) and triple-positive (**f**) cells is shown. 3 donors with duplicates. Student's t-test, *P < 0.05.

(**g–i**) Effects of GSK126 on H3K27me3 expression and polyfunctionality in $CD8^+$ T cells. T cells were stimulated with anti-CD3 and anti-CD28 antibodies for 4 days. 10 μM GSK126 was added on Day 0 and 2. The expression of EZH2, H3K27me3, H3, and β-actin was detected with immunoblotting in 3 donors with duplicates (**g**). Expression of IFN-γ, TNF, and granzyme B was analyzed by flow cytometry. The percentage of double (**h**) and triple-positive (**i**) cells is shown (mean ± SEM, N = 5, Wilcoxon rank-sum, *P < 0.05).

(**j**) Effects of EZH2 on T cell apoptosis. T cells were treated with 5 μM DZNep, 10 μM GSK126 or shEZH2 transfection and activated with anti-CD3 and anti-CD28 antibodies for 2 days. T cell apoptosis was evaluated with Annexin V and 7-AAD staining. Representative dotplots for one of 5 donors tested.

(**k,l**) Effects of EZH2 blockade on Bcl-2 expression. T cells were treated with 5 μM DZNep or shEZH2 transfection and activated for 3 days. Expression of Bcl-2, EZH2, and β-actin was detected with immunoblotting. One of 5 experiments is shown.
(**m**) Effect of EZH2 blockade on Bcl-2 promoter activity. 293T cells were co-transfected with vectors encoding shEZH2 or scramble and hBCL-2-EGFP vector for 2 days. The promoter activity was analyzed by flow cytometry and expressed as the percentage of GFP expression (mean ± SD). N = 4, *P < 0.05.

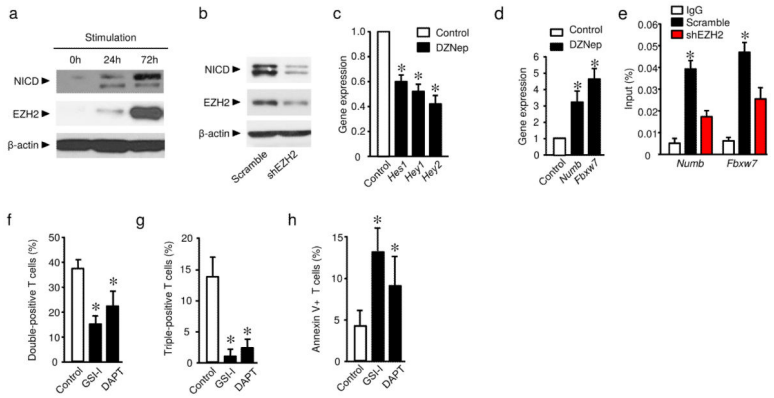

Fig. 3. EZH2 inhibits Notch repressors, T cell polyfunctionality, and survival

(**a**) Kinetic activation of EZH2 and Notch in T cells. T cells were stimulated with anti-CD3 and anti-CD28 antibodies for the indicated time. Expression of NICD, EZH2, and β-actin was detected with immunoblotting. One representative experiment of 3 is shown.

(**b**) Effect of EZH2 blockade on Notch activation. ShEZH2 lentivirus transfected T cells were activated for 3 days. Expression of NICD, EZH2 and β-actin was detected with immunoblotting. One representative experiment of 3 experiments is shown.

(**c,d**) Effect of DZNep on Notch signaling gene expression. Human T cells were activated in the presence of 5 μM DZNep for 2 days. Expression of active Notch signaling genes (*HES1*, *HEY1*, and *HEY2*) (**c**), and Notch repressor genes (*NUMB* and *FBXW7*) (**d**) was quantified by real-time PCR. Results are expressed as the relative expression (mean ± SD). N = 5, Wilcoxon test, *P < 0.05.

(**e**) H3K27me3 binding to the proximal promoter areas of *NUMB* and *FBXW7*. Jurkat cells were transfected with shEZH2 or scramble. ChIP assay was performed with anti-H3K27me3 antibody. The occupancy of H3K27me3 in the proximal promoter areas of *NUMB* and *FBXW7* was examined and expressed as the percentages of input (mean ± SEM). N = 4 transfections, each in triplicate, Wilcoxon test, *P < 0.05.

(**f–h**) Effects of Notch signaling inhibition on T cell polyfunctionality and apoptosis. $CD8^+$ T cells were activated with anti-CD3 and anti-CD28 in the presence of two gamma-secretase inhibitors: DAPT and GSI-I. Polyfunctionality (**f,g**) and apoptosis (**h**) were analyzed by flow cytometry. Data from 3 donors are shown (mean ± SEM). Mann-Whitney U test, *P < 0.05.

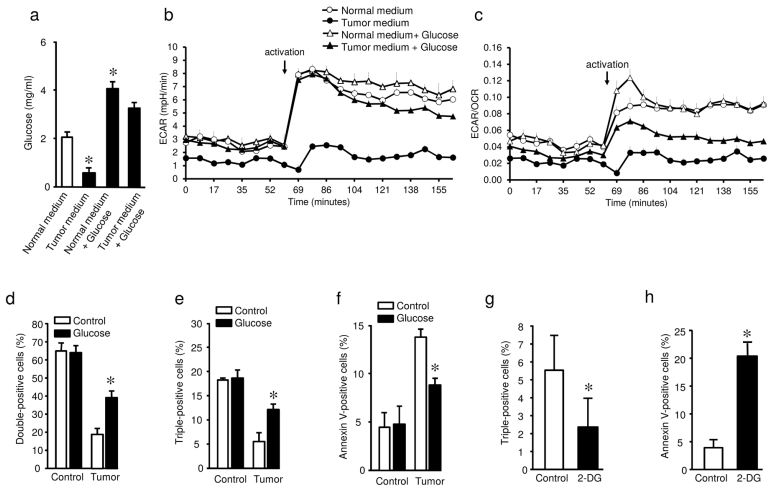

Fig. 4. Tumor impairs T cell polyfunctionality and survival via glucose restriction

(**a**) The concentrations of glucose in different culture media. Glucose was detected in normal medium, primary ovarian cancer cell medium, and these two media supplemented with additional glucose. Tumor medium was supplemented with an additional 2 mg/ml glucose after culture with tumor cells. Results are shown as mean ± SEM, N = 4, Wilcoxon rank-sum test, *P<0.05.

(**b,c**) Metabolic profile of normal and tumor-conditioned memory $CD8^+$ T cells. Memory $CD8^+$ T cells were pre-incubated overnight in medium or tumor-conditioned supernatants with or without glucose supplementation, and activated with anti-CD3 and anti-CD28. ECAR (**b**) and ECAR/OCR ratio (**c**) were assayed in different time points in a Seahorse XF24 analyzer. Results are shown as the mean value from four repeats for each treatment ± SEM. Representative data from one of 4 independent experiments on 4 different donors.

(**d–f**) Effects of tumor associated glucose restriction on $CD8^+$ T cell polyfunctionality and apoptosis. Memory $CD8^+$ T cells were pre-incubated overnight in medium or tumor-conditioned supernatants with or without glucose supplementation and washed and stimulated for 48 hours with anti-CD3 and anti-CD28 antibodies. Polyfunctional profile was analyzed by flow cytometry. Results are shown for double-positive (**d**) and triple-positive (**e**) cells for IFN-γ, TNF, and granzyme B. T cell apoptosis (**f**) was determined by Annexin V staining and analyzed by flow cytometry. Results are shown as the mean ± SEM in 4 donors. Mann-Whitney U test, *P < 0.05.

(**g,h**) Effects of 2-DG on $CD8^+$ T cell polyfunctionality and apoptosis. $CD8^+$ T cells were activated with anti-CD3 and anti-CD28 for 3 days in the presence or absence of 2-DG. Polyfunctionality (**g**) and Annexin V binding (**h**) were assessed by flow cytometry. Results are shown as the mean ± SD of 4 donors. Wilcoxon rank-sum test, *P < 0.05.

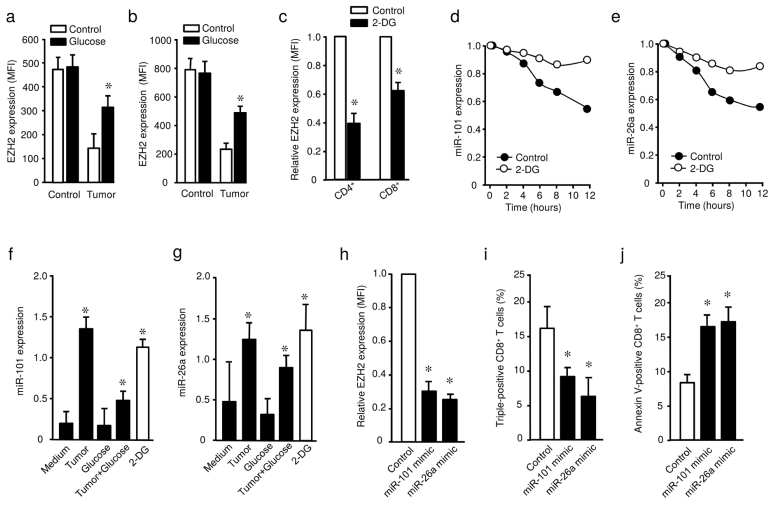

Fig. 5. Tumor controls T cell EZH2 by microRNA101 and microRNA26 via glucose restriction

(**a,b**) Effect of tumor associated glucose restriction on T cell EZH2 expression. $CD4^+$ (**a**) and $CD8^+$ (**b**) T cells were activated with anti-CD3 and anti-CD28 for 3 days in medium or tumor conditioned medium with or without glucose supplementation. EZH2 protein expression was determined by flow cytometry. Results are shown as the mean fluorescence intensity (MFI) of EZH2 ± SEM in 3 donors, Mann-Whitney U test, *P < 0.05

(**c**) Effect of 2-DG on T cell EZH2 expression. T cells were activated with anti-CD3 and anti-CD28 for 3 days in the presence or absence of 2-DG. EZH2 protein expression was determined in viable T cells by flow cytometry. Results are shown as the relative EZH2 expression to the control group ± SEM in 3 donors, Mann-Whitney U test, *P<0.05.

(**d,e**) Dynamic changes of microRNA101 and microRNA26a in activated $CD8^+$ T cells. $CD8^+$ T cells were activated with anti-CD3 and anti-CD28 in the presence or absence of 2-DG. MicroRNA101 (**d**) and microRNA26a (**e**) were measured by qPCR in different time points. Results are shown as the relative microRNA expression. One of 2 donors is shown.

(**f,g**) Effect of tumor associated glucose restriction on microRNA expression in $CD8^+$ T cells. Memory $CD8^+$ T cells were pre-incubated overnight in medium or tumor-conditioned supernatants with or without glucose supplementation, then washed and stimulated for 12 hours with anti-CD3 and anti-CD28 antibodies. The abundance of microRNA101 (**f**) and microRNA26a (**g**) was measured by qPCR. Data are presented as the mean ± SEM, N = 3, Mann-Whitney U test, *P < 0.05.

(**h–j**) Effects of microRNA mimics on T cell EZH2 expression, polyfunctional profile, and apoptosis. Memory $CD8^+$ T cells were nucleofected with microRNA101 mimic, micorRNA26a mimic, or control oligonucleotide, and activated with anti-CD3 and anti-CD28 for 48 hours. T cell EZH2 expression (**h**), polyfunctionality (**i**), and apoptosis (**j**) were determined by flow cytometry. Results are shown as the relative mean of EZH2 expression (**h**), the mean percentage of triple positive T cells (**i**), and the mean of Annexin V^+ cells (**j**) ± SEM, N = 4, Mann-Whitney U test, *P < 0.05.

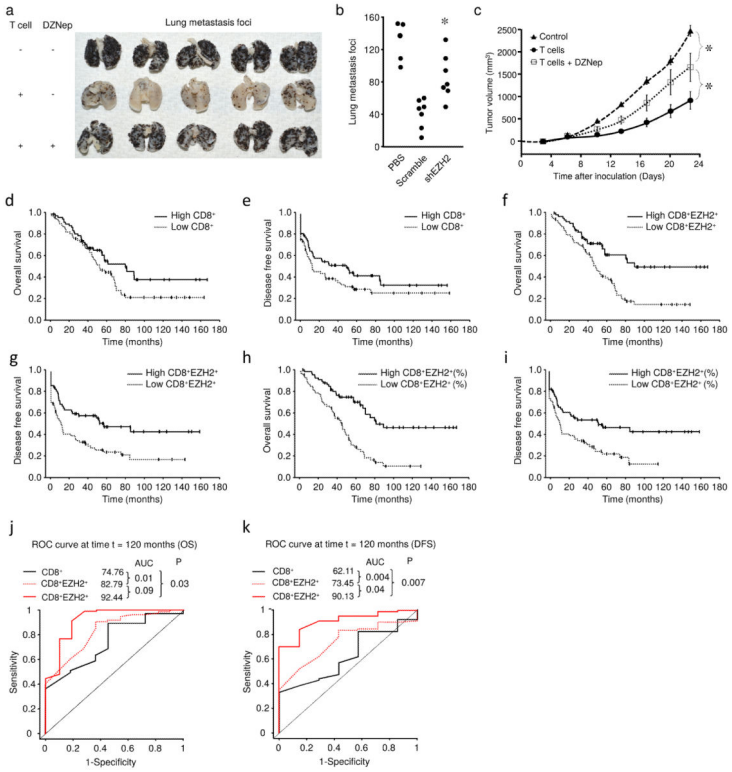

Fig. 6. EZH2 affects T cell-mediated anti-tumor immunity and patient survival

(**a**) Effects of biochemical blockade of T cell EZH2 on mouse melanoma metastasis. Melanoma cells were intravenously injected into C57BL/6 mice to induce lung metastasis. Tumor specific T cells were activated in the presence or absence of 1 μM DZNep for 2 days and expanded in IL-2 for 3 days. These T cells were intravenously transfused into tumor-bearing mice. Lung metastatic loci were counted on day 16. N = 15 mice total, 5 per group, all individuals shown.

(**b**) Effects of genetic blockade of T cell EZH2 on mouse melanoma metastasis. Tumor specific T cells transfected with lentiviral vector expressing shEZH2 or scramble were activated for 2 days and expanded in IL-2 for 3 days. These T cells were intravenously transfused into tumor-bearing mice. Lung metastatic loci were counted on day 16. N = 5–7 per group, each dot represents individual mouse. Mann-Whitney U test, *P < 0.05 (shEZH2 compared to scramble).

(**c**) Effects of T cell EZH2 blockade on human ovarian cancer growth. Human primary ovarian cancer cells were subcutaneously injected into female NOD/Shi-scid/IL-2Rγ^{null} (NSG) mice. Tumor-specific T cells were initially treated with or without 1 μM DZNep *in vitro* and were intravenously transferred into ovarian cancer bearing NSG mice. Tumor volume was measured. Results are expressed as the tumor volume (mean ± SEM). N = 5 mice per group, Mann-Whitney U test, *P < 0.05.

(**d–i**) Tumor infiltrating T cells and patient outcome. Ovarian cancer tissue microarray was subject to immunohistochemistry staining with anti-CD8 and anti-EZH2 antibodies. $CD8^+$ and $EZH2^+CD8^+$ T cells were quantified. Kaplan–Meier estimates of overall survival and progression-free interval were performed according to the median values of $CD8^+$ T cell numbers (**d,e**), $EZH2^+CD8^+$ T cell numbers (**f,g**), and the percentage of $EZH2^+CD8^+$ T cells

(**h,i**). Kaplan-Meier estimates are shown in Supplementary Tables 1–3.
(**j,k**) Relative impact of $CD8^+$ T cell numbers, $EZH2^+CD8^+$ T cell numbers, and the percentage of $EZH2^+CD8^+$ T cells on patient long-term survival. The time-dependent receiver operating characteristic (ROC) curve analysis was applied to evaluate the predictive accuracy of each marker for a 10-year overall survival (OS) (**j**) and disease free survival (DFS) (**k**). AUC, the area under the ROC curve.